A PURE VORTEX METHOD FOR SIMULATING UNSTEADY, INCOMPRESSIBLE, SEPARATED FLOWS AROUND STATIC AND PITCHING AEROFOILS

Hequan Lin and Marco Vezza [1]
Department of Aerospace Engineering
University of Glasgow

Abstract

Through the representation of vorticity fields by discrete vortices, the vortex method has shown its suitability in simulating vortex dominated flows, such as those surrounding bluff bodies. However, for a streamlined body like an aerofoil, the method has had to resort to other grid dependent schemes to locate separation points. In this paper, a pure vortex model is presented to solve the Navier-Stokes equations in vorticity/stream function form, integrating the influence of moving boundaries. The flow region is divided into creation and wake zones, and the model adopts a different discretization procedure in each zone. The exchange of vorticity between zones is simulated in accordance with the vortex positions relative to the body surface after the advance of time. The nascent vorticity is obtained from the implementation of appropriate boundary conditions to a multi-panel representation of the body surface. The results of the application of this pure vortex method to static and pitching aerofoils illustrate that it is able to predict separation and reattachment, while the comparison of predicted aerodynamic characteristics with experimental data shows good agreement.

Introduction

Like other numerical simulation models, vortex modelling has been the subject of research in numerous publications the during last few dacades. Its continous and substantial progress has been comprehensively summarized in review papers[1],[2].

The representation of vortical regions in incompressible flows by discrete vortices enables the concentration of computing resources only in areas of non-zero vorticity. In addition the flexibility arising from this grid free scheme makes it especially suitable for numerical simulation of flows in which the boundaries are moving continously, for example the flows around a pitching aerofoil.

In potential flow applications of the vortex method, a vortex appears as a singular element, introduced wherever a sudden velocity change exists, with the associated velocity field obtained from the Biot-Savart law. The flow around a static aerofoil at low angle of attack can be modelled in this way. Traditionally a singular element vortex sheet is placed on the surface, the strength of which is determined from the implementation of no penetration through the surface in conjunction with the trailing edge Kutta condition. This leads to a solution of the Euler equations, however the capability of the method can be broadened by the introduction of vortex blobs and the incorporation of models to integrate diffusion effects caused by viscosity. The vortex core eliminates the infinite induced velocities, and the random walk scheme[3] and vortex strength exchange model[4] extend the applicability of the method to a wide range of incompressible flows described by the Navier-Stokes equations. The accuracy and convergence of the schemes have also been addressed by several publications[5],[6].

The interest in vortex evolution schemes involving convection and diffusion of vorticity has arisen as a consequence of the close resemblance between computed vortex structures and those obtained from experimental research on bluff bodies and aerofoils. These encouraging results, however, often pertain to flows in which the location of separation points are fixed by sharp edges or are known in advance. Other than for attached flows leaving the trailing edge, such advantages do not exist in flows around streamlined bodies like aerofoils, for which separation points cannot be pre-defined. To identify such points, workers have often resorted to other numerial schemes, like the finite element method[7], within the boundary layer. This has actually returned the method back to grid reliance in conjunction with artificial suppression of vortex release in unseparated areas to maintain a smooth solution for the pressure distribution.

Interest in research into flows around pitching aerofoils arose from the perceived potential benefits in the improved performance of fighters, helicopters and wind turbines. From the experimental research results, these unsteady flows with moving boundary are dominated by a vortex, known as the dynamic stall vortex. In addition to the vortex method, some grid based schemes like the O-grid scheme combined with the Joukowsky transformation[8]; the Moving O-grid scheme[9]; the hybrid grid scheme (dynamic structured and unstructured grid)[10]; viscous/inviscid interaction schemes[11]; the random walk vortex method coupled with the Von Mises transform[12], have been able to predict the flows numerically. Of all these, the capability of the vortex method will be greatly enhanced by developing a model which can decouple its reliance on other

[1] Department of Aerospace Engineering, University of Glasgow, Glasgow, G12 8QQ, UK

schemes in prediction of separation points. To achieve this is a major task of the present research.

In this paper, a pure vortex model is presented to integrate the influence of moving boundaries and to solve the vorticity/stream function form of the Navier-Stokes equations. The flow region is divided into a creation zone and wake zone, with different discretization procedures adopted for each. Within the creation zone vortices are located at discrete points which are fixed with respect to the body, and changes in vortex strength are in accordance with the requirement of the no slip/no penetration boundary conditions. In the wake zone, the strength of an individual vortex remains constant, with its position determined by convection and a perturbation consistent with the random walk method to simulate diffusion effects. The exchange of vorticity between the two flow zones is dependent on the vortex positions relative to a multi-panel representation of the body surface, after the advance of time. The results of the application of this pure vortex method to static and pitching aerofoils illustrate the ability to predict separation and, where appropriate, reattachment. In addition the comparison of predicted aerodynamic characteristics with experimental data shows good agreement.

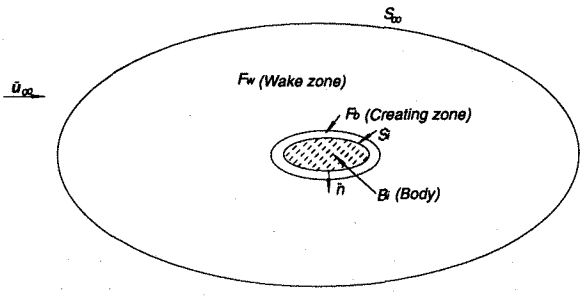

Figure 1. Flow domain

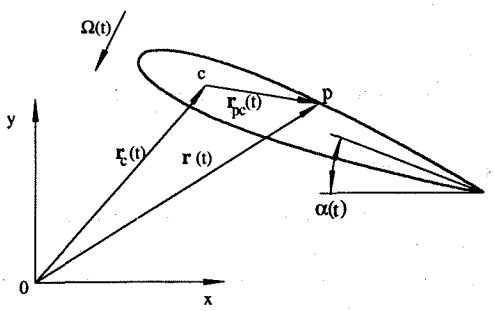

Figure 2. Reference coordinate system

Governing Equations

Velocity/pressure form

Two dimensional incompressible flow, depicted in figure 1, is governed by the following continuity and full viscous Navier-Stokes equations:

$$\nabla . \vec{u} = 0 \tag{1}$$

$$\frac{D\vec{u}}{Dt} = -\frac{1}{\rho} \nabla P + \nu \nabla^2 \vec{u} \tag{2}$$

where $\vec{u}$ is the flow velocity, ρ is the fluid density, P is the static pressure, t is the time and ν is the kinematic viscosity.

Their solutions are subjected to boundary conditions

$$\vec{u} = \vec{u}_i \text{ on } S_i \text{ and } \vec{u} = \vec{u}_\infty \text{ on } S_\infty \tag{3}$$

which means that flow in the far field is undisturbed and the velocity of each flow particle is equal to that of the body at the surface due to the no-slip/no-penetration conditions.

Without deformation, the body surface velocity corresponds to that of a solid region with reference point c, depicted in the figure 2,

$$\vec{u}_i = \vec{u}_{ic} + \vec{\Omega}_i \times (\vec{r} - \vec{r}_{ic}) \tag{4}$$

where subscript i is the index for the body, $\vec{u}_{ic}$ is the velocity of its reference point, and $\vec{\Omega}_i$ is the angular velocity.

Vorticity/stream function form

By using the definitions of vorticity $\vec{\omega} = \nabla \times \vec{u}$ with $\vec{\omega} = \vec{k}\omega$, vector potential $\vec{\Psi}$ with $\vec{u} = \nabla \times \vec{\Psi}$, $\vec{\Psi} = \vec{k}\Psi$, $\nabla . \vec{\Psi} = 0$, and rotational velocity $\vec{\Omega}_i = \vec{k}\Omega_i$, the governing equations can be expressed in vorticity/stream function form:

$$\nabla^2 \Psi = -\omega \tag{5}$$

$$\frac{D\omega}{Dt} = \nu \nabla^2 \omega \tag{6}$$

and the boundary conditions are

$$\nabla\Psi = \nabla\Psi_i \text{ on } S_i \text{ and } \nabla \Psi = \nabla\Psi_\infty \text{ on } S_\infty \tag{7}$$

where, on S_i, Ψ_i satisfies

$$\Psi_i = \vec{k}.[\vec{u}_{ic} \times (\vec{r} - \vec{r}_{ic})] + \frac{1}{2}\Omega_i |\vec{r} - \vec{r}_{ic}|^2 + constant$$

a solution of

$$\nabla^2 \Psi_i = -2\Omega_i \tag{8}$$

defined over area B_i occupied by solid body i with the same conditions on S_i.

Velocity vs vorticity

The relationship between the velocity and the vorticity has been derived by the application of Green's Theorem to (5) for region F and (8) for B_i, and combining them through the boundary conditions. For a point p outside the solid region, the result is

$$\vec{u}_p = \vec{u}_\infty + \frac{1}{2\pi} \int_{F_b} \omega \frac{\vec{k} \times (\vec{r}_p - \vec{r})}{\|\vec{r}_p - \vec{r}\|^2} dF_b$$

$$+ \frac{1}{2\pi}\int_{F_w} \omega \frac{\vec{\mathbf{k}} \times (\vec{\mathbf{r}}_p - \vec{\mathbf{r}})}{\|\vec{\mathbf{r}}_p - \vec{\mathbf{r}}\|^2} dF_w$$
$$+ \frac{1}{2\pi}\int_{B_i} 2\Omega_i \frac{\vec{\mathbf{k}} \times (\vec{\mathbf{r}}_p - \vec{\mathbf{r}})}{\|\vec{\mathbf{r}}_p - \vec{\mathbf{r}}\|^2} dB_i \qquad (9)$$

where $F = F_b \cup F_w$ and $F_b \cap F_w = 0$.

The equation details the four contributions to the velocity from the free stream, the vorticity in the small control area F_b around the solid region (creation zone), the vorticity in the remaining flow area F_w, and the equivalent vorticity inside the solid region due to the motion of the body. The equation also indicates the means by which knowledge about vorticity fields leads to knowledge of velocity fields.

Numerical Implementation

Surface representation

For a two dimensional body, as illustrated in figure 3, a polygonal representation of the body surface is created by connecting node points with a straight line to form a series of panels. N main node points are located on the body which define N plane panels approximating the N curved segments of the surface. Each curved segment is further subdivided into n equal length sub-panels by the specification of $n-1$ nodes along the segments.

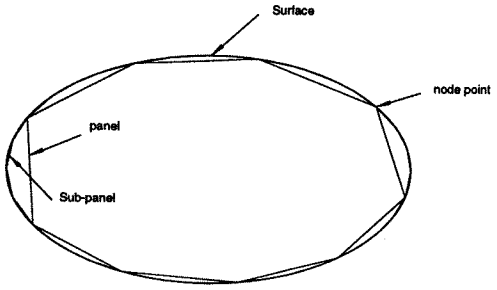

Figure 3. Multi-panel representation

Vorticity Discretization

The entire flow region is divided into two sub-regions, each with a different vorticity discretization procedure. The thin layer near the body surface is regarded as a special zone, the creation zone, in which the vorticity is produced. The vorticity in the rest of the flow field arises through convection and diffusion of that generated in the creation zone.

The thinness of the creation zone makes it acceptable to reduce the vorticity field to a one dimensional vortex sheet, which is then discretized into vortices in a two stage process in accordance with the surface representation.

Firstly, the sheet strength, γ, is treated as a quantity which varies piecewise linearly and continuously along the surface. The values of γ at main node points therefore represent the entire vorticticiy distribution within the creation zone.

Secondly, the panel distribution of vorticity is further broken down into vortex blobs, one for each sub-panel. The blob is positioned a distance δ directly above the middle of the sub-panel. The discretization is illustrated in figure 4

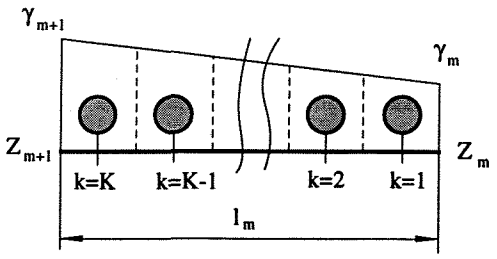

Figure 4. Discretization and γ distribution

The relative position of the vortices to the body is fixed, while circulation changes are reflected in the γ distribution.

In the other sub-region, wake zone F_w, vorticity is discretized into vortices in accordance with the final step of the previous discretization. The process can be regarded as one of an individual vortex advancing in time, through convection and diffusion, with the same circulation. This corresponds to solving the vorticity transport equation after operator splitting. The convection velocity is equal to that of the associated particle and can be evaluated by equation (9), where the integrals are replaced by summations due to the discretization of the vorticity field. The Adams-Bashforth second order method is employed to locate the convected position, to which additional displacements, η_x, η_y in the x and y directions, are added to simulate viscous diffusion. These displacements are generated through the random walk method and satisfy the Gaussian distribution of zero mean and standard deviation $\sqrt{2\Delta t/Re}$. Accordingly a discrete point of $z_i(t)$ at instant of time t shifts to

$$(z_i(t+\Delta t))_w = z_i(t) + \left[\frac{3}{2}V_i(t) - \frac{1}{2}V_i(t-\Delta t)\right]\cdot\Delta t + (\eta_x + i\eta_y) \qquad (10)$$

at $t+\Delta t$ while the advance of each creation zone vortex is

$$(z_i(t+\Delta t))_c = z_i(t) + V_i(t)\cdot\Delta t + (\eta_x + i\eta_y) \qquad (11)$$

The exchange of vorticity between the two zones, or the release and absorption of vortices from/to the wake zone are determined by the new vortex positions at the next instant of time, with respect to the surface position. At the beginning of the calculation, the total number of such vortices is zero, as is the mass flow contribution.

Surface vorticity determination

The γ values in the creation zone are the solution of equations from the boundary condition which is implemented by ensuring zero mass flow through each surface panel. Although this does not guarantee that the equations are satisfied at every point, there is at least one point on each panel with zero relative normal velocity. The implementation is expressed as

$$F_{js} + F_{ji} + F_{jf} + F_{jv} + F_{jn} = 0 \qquad (12)$$

with each term representing the contribution of mass flow from different sources. The first and second terms F_{js}, F_{ji} are from the motion of the body and are thus additional items to those for the static case. F_{jf}, F_{jv} and F_{jn} represent the contributions from the free stream, the vortices in the wake and the vortices within the creation zone.

The total number of equations (12) is N for a body with N panels, but only $N-1$ are independent because there is no source or sink within the body. Hence when $N-1$ panels satisfy zero mass flow, the mass flow for the final panel will automatically be zero.

A further equation required to make the solution unique is obtained from the requirement for a single-valued pressure field, and results in a circulation condition. For each body, the additional condition is

$$\sum_v \Gamma_v + \sum_{m=1}^{N}\sum_{k=1}^{K} (\Gamma_m)_k + 2\Omega_i A_i = \Gamma_{st} \qquad (13)$$

where the first term is the circulation of vortices in the wake, the second is the circulation of vortices in the creation zone, the third is the circulation due to the body rotation and the fourth is the initial circulation in the flow field prior to the start of calculations. The second term contains the unknown γ values.

Pressure evaluation

Operating with $\vec{\mathbf{n}}\times$ on the N-S equation (2) applied to the body surface, an equation for pressure gradient is obtained

$$\frac{1}{\rho}\frac{\partial P}{\partial s} = -\vec{\mathbf{s}}.\frac{D\vec{\mathbf{u}}}{Dt} + \nu\frac{\partial \omega}{\partial n} \qquad (14)$$

where $\vec{\mathbf{n}}$, the normal vector, and $\vec{\mathbf{s}}$, the tangential vector are related by $\vec{\mathbf{n}} = \vec{\mathbf{s}} \times \vec{\mathbf{k}}$.

Because of the no-slip condition the flow velocity on the surface should be the same as that of the surface itself, given by (4). Hence the equation becomes (dropping index i)

$$\begin{aligned}\frac{1}{\rho}\frac{\partial P}{\partial s} &= -\vec{\mathbf{s}}.\frac{D\vec{\mathbf{u}}_c}{Dt} - \vec{\mathbf{n}}.\left(\vec{\mathbf{r}}-\vec{\mathbf{r}}_c\right)\frac{D\Omega}{Dt} \\ &+ \vec{\mathbf{s}}.\left(\vec{\mathbf{r}}-\vec{\mathbf{r}}_c\right)\Omega^2 + \nu\frac{\partial \omega}{\partial n} \qquad (15)\end{aligned}$$

The first three terms on the right hand side of the above equation only appear when the body is in motion and they describe the surface tangential components of the acceleration of the reference point, the rotational acceleration and the centripetal acceleration.

Rewriting the vorticity transport equation (5) as

$$\frac{D\omega}{Dt} = \frac{\partial \omega}{\partial t} + \left(\vec{\mathbf{u}}.\nabla\right)\omega = -\nabla.(-\nu\nabla\omega) \qquad (16)$$

$-\nu\nabla\omega$ is the vorticity flux which, when applied at the body, produces the surface flux $-\vec{\mathbf{n}}.\nu\nabla\omega = -\nu\partial\omega/\partial n$. Therefore the last term in (14) can be regarded as the negative vorticity creation rate at the surface.

Consider a control area with one side on part of the body surface and the opposite side on the upper part of the control zone, figure 5. The control area has size ds along the surface and moves with the body. The circulation of vortices inside the control area at time t, excluding the vorticity created by the surface at this time, is $\gamma^a ds$. This includes the vorticity in existence there at time $t-\Delta t$ and the vorticity flux through the area boundaries (excluding the body surface) from $t-\Delta t$ to t. The circulation of vortices created at the element of surface during this time step is $\left(-\nu\partial\omega/\partial n\right) ds\Delta t$. The nett circulation of vortices inside this area, γds, is given by the sum of these contributions, that is

$$\left(-\nu\frac{\partial\omega}{\partial n}\right) ds\Delta t + \gamma^a ds = \gamma ds \qquad (17)$$

so

$$\nu\frac{\partial\omega}{\partial n} = \frac{\gamma^a - \gamma}{\Delta t} \qquad (18)$$

where γ^a is the equivalent circulation density of existing vortices in the control area at time t, and is approximated piecewise linearly in the same fashion as the nett vorticity γ.

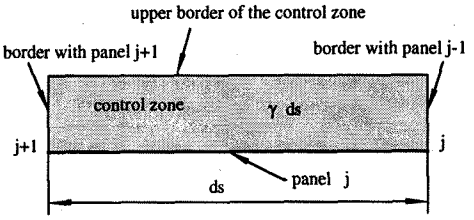

Figure 5. Vorticity inside the control zone

The integrals from pressure gradient to pressure distribution and from the pressure to aerodynamic force and moment are standard.

Results and Analysis

The model has been used to predict some attached and separated flows. The results for starting flow around a NACA0012 undergoing various motions are presented below, including impulse start, ramp-up motion and ramp-up ramp-down triangle motion.

Case 1:$\alpha = 5°$, $\alpha = 8°$, $\alpha = 10°$ impulse start unsteady static flows (attached flows)

Figure 6 illustrates the vortex patterns and surface pressure distributions for these cases, the first two frames corresponding to times shortly after the impulse start and after the flow around the aerofoil has settled at 10°. The rest are for settled flows at 5° and 8° respectively. The Reynolds numbers are $Re = 990000$. From the earlier frame, the vortices are seen to be emitting from the trailing edge and rolling up. This represents the starting vortex and during this period circulation is built up around the airfoil and the suction near the leading edge is relatively small. The later frames show the settled vortex patterns, with vortices again emitting from the trailing edge but no longer rolling up. This is due to the vortices trailing from both the upper and lower surfaces being of opposite sign and almost the same magnitude. At this stage there is little overall change in the circulation around the airfoil. Also evident is the close proximity of the emerging vortices to the aerofoil surface although the layer where vortices appear on the upper surface is thicker than that at the smaller angles. This is in good accordance with the established knowledge that the steady flows for these cases are attached and the further increase of angle of attack will lead to flow separation. Velocity vectors and stream lines in figure 7 of the settled flow around the 10° aerofoil show again the attached flow.

The time histories of the normal force and pitching moment coefficients C_n *vs* $t \times V/c$ (dimensionless time), $C_{m1/4}$ *vs* $t \times V/c$ are presented in figure 8. These illustrate the classic features of starting flow, i.e. an initial impulse followed by a gradual build up to steady state values corresponding to the increasing circulation which develops around the aerofoil. This process is consistent with the frames in figure 6 where the starting vortex can be seen to be carrying circulation downstream. The circulation around the body surface increases to maintain constancy of total circulation.

Also in figure 8 is the experimental C_n, which has been reduced from published steady state test data[13]. From this figure it is apparent that, after the initial transient has died away, the predicted C_n approaches very close to the test result.

Case 2: ramp-up

Four frames are presented in figure 9 for the case of a ramp change in angle of attack from $-1°$ to 40°, at $Re = 1020000$ and reduced pitch rate $k = 0.0415$. The starting and ending phases of the motion are modelled as an acceleration and deceleration, as shown in figure 11, in which the time history is the same as that for the experiment. The first frame shows the attached flow at an angle of 16.5°, higher than the static stall value. In the second frame, in which dimensionless time $t \times V/c = 7.0$, and $\alpha = 21.5°$, the main dynamic vortex is formed near the leading edge upon the upper surface and correspondingly the suction pressure is increased there. In addition the secondary and tertiary group of vortices can be seen to be formed on other portions of the upper surface. They

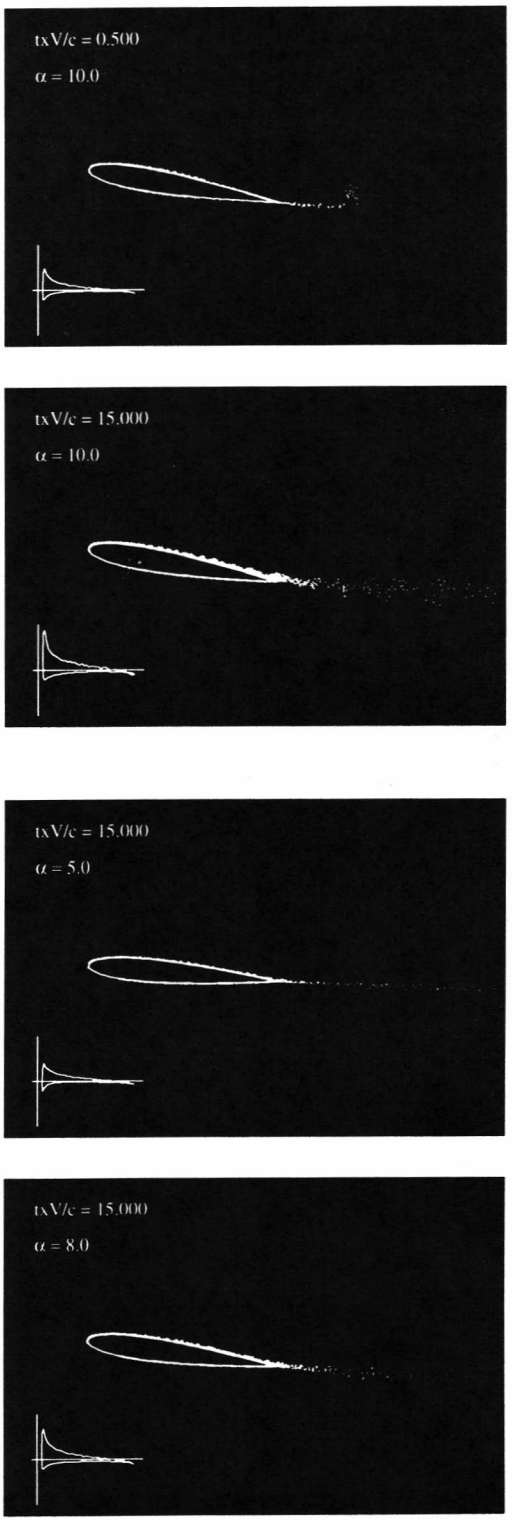

Figure 6. Vortex pattern and pressure distribution of the NACA0012 in impulsive flow at $\alpha = 10°, \alpha = 5°, \alpha = 8°$

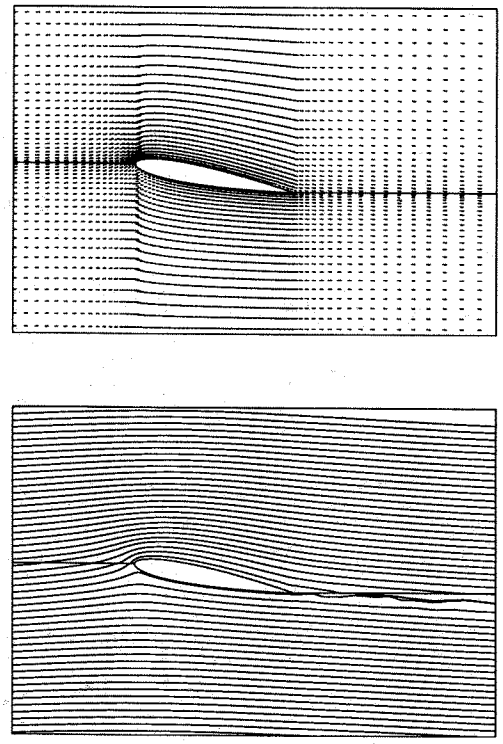

Figure 7. Velocity field and streamlines of the settled flow at $\alpha = 10°$

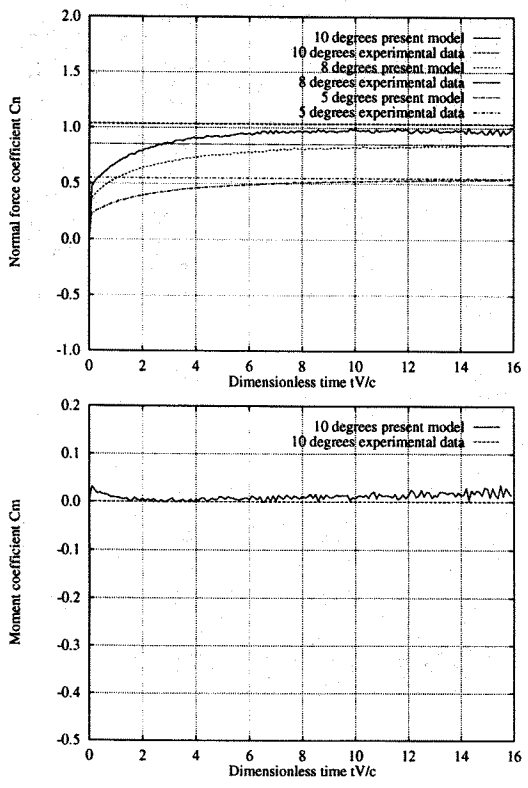

Figure 8. Aerodynamic characteristics

combine together to develop a secondary dynamic vortex as shown in the third frame, where the dominant effect of the main dynamic vortex in the pressure distribution is apparent. The main vortex absorbs the secondary vortex and sweeps downward along the surface. As it is about to leave the trailing edge, a counter vortex is formed there, which can be seen in the fourth frame. The corresponding velocity fields in figure 10 give another insight to these events.

Angle of attack α time history, C_n *vs* $t \times V/c$ (dimensionless time) and $C_{m1/4}$ *vs* $t \times V/c$ are presented in figure 11, together with the test results[14]. Good agreement can be seen until $t \times V/c = 7.0$, which corresponds to about $\alpha = 21.5°$. After that, the model predicts slightly higher C_n and there is a difference in the peak C_n also. This means the model predicted an earlier separation than the experiment. This might be due to the core function and turbulent influences. These may also be the contributors to the difference in C_n and $C_{m1/4}$ afterwards. The peak difference may also be due to the wind tunnel blockage influence as the test data was not subject to wind tunnel correction.

Case 3: ramp-up and ramp-down

In figure 12 are four frames for ramp-up and ramp-down, with two for each motion stage. They are accompanied by corresponding streamline pictures in figure 13 and by the angle of attack α time history, C_n *vs* $t \times V/c$, $C_{m1/4}$ *vs* $t \times V/c$ in figure 14. The angle of attack is increased from 0° to 40° and then is reduced to $-10°$ at reduced pitch rate $k = 0.0487$ for each case. Reynolds number $Re = 990000$. Frame one shows the flow is still attached at high angles of attack, and the second frame presents the separation from the leading edge during the pitching up process. Frame three shows the separation point is moving rearward and the final frame illustrates the flow fully attached.

The characteristic hystereses in the aerodynamic loads are predicted. Of particular importance is the reduction in C_n during ramp down. During ramp-up the processes are virtually identical to those described in the previous case. However the delay in reattachment and lack of vortex lift during ramp-down results in lower C_n values. Although upper surface suction starts to build up during ramp-down at higher incidence, this process is undermined by the continual reduction in incidence and possibly by the influence of the vortex system previously shed.

Conclusions

A discrete vortex model has been developed which is able to predict separated, incompressible flows without resorting to other schemes for separation points. The agreement with test data shows the introduction of the creation zone around the body and the different discretization procedure for its vorticity has enabled the modelling of separated flows, like those around pitching aerofoils. It is anticipated that future developments, in particular the incorporation turbulence effects, will further improve the prediction capabilities of the model.

Acknowledgements

The authors would like to thank Prof R.A.McD. Galbraith for his consistant encouragement, Dr. F.Coton, Dr. R.Green of the Department for their friendly and very useful discussion and Mrs E. leitch for her assistance in obtaining the test data. First author also acknowledges the CVCP for its financial support through the ORS Awards scheme.

References

[1] Sarpkaya, T. 1989. "Computational Methods With Vortices - The 1988 Freeman Scholar Lecture".

[2] Leonard, A. 1985. "Computing three-dimensional incompressible flows with vortex elements". Ann. Rev. Fluid Mech. 17, 523.

[3] Chorin, A.J., "Numerical study of slightly viscous flow". Journal of Fluid Mech., 57(4), 1973, pp785-796.

[4] Fishelov, D., "A New Vortex Scheme for Viscous Flows". Journal of Computational Physics, Vol. 86, 1990, pp. 211-224.

[5] Perlman, M., "On the Accuracy of Vortex Methods". Journal of Computational Physics, Vol. 59, 1985, pp200 - 223.

[6] Sethian, J. A., and Ghoniem, A. F., "Validation Study of Vortex Methods". Journal of Computational Physics, Vol. 74, 1988, pp283-317.

[7] Spalart, P. R. 1988. "Vortex Methods for Separated Flows". NASA TM 100068

[8] Tuncer, I. H., Wu, J. C., and Wang, C. M. "Theoretical and Numerical Studies of Oscillating Airfoils". AIAA Journal, Vol. 28, No. 9, Sept. 1990. pp1615-1624.

[9] Visbal, M. R. "Dynamic Stall of a Constant-Rate Pitching Airfoil". Journal of Aircraft, Vol. 27, No. 5, May, 1990. pp400-407.

[10] Reu, Taekyu, and Ying, S. X. "Hybrid Grid Approach to Study Dynamic Stall". AIAA Journal, Vol. 30, No. 11, Nov. 1992, pp2670-2676.

[11] Tuncer, I. H., Ekaterinaris, J. A., and Platzer, M. F. "Viscous/Inviscid Interaction Method for Unsteady Low-Speed Airfoil Flows" AIAA Journal Vol. 33, No. 1, Jan. 1995.

[12] Shih, C., Lourenco, L., VanDommelen, L., Krothapalli, A. "Unsteady Flow Past an Airfoil Pitching at a Constant Rate". AIAA Journal, Vol. 30, No. 5, May, 1992.

[13] Abbott, I.H., and Doenhoff, A.E.V. "Theory of Wing Sections". Dover Publications, Inc, 1959.

[14] Galbraith, R.A.McD., Gracey, M.W., and Gilmour, R. "Collected data for tests on a NACA 0012 Aerofoil". Volume I: Pressure data from ramp function tests. G.U. AERO report 9207, February, 1992..

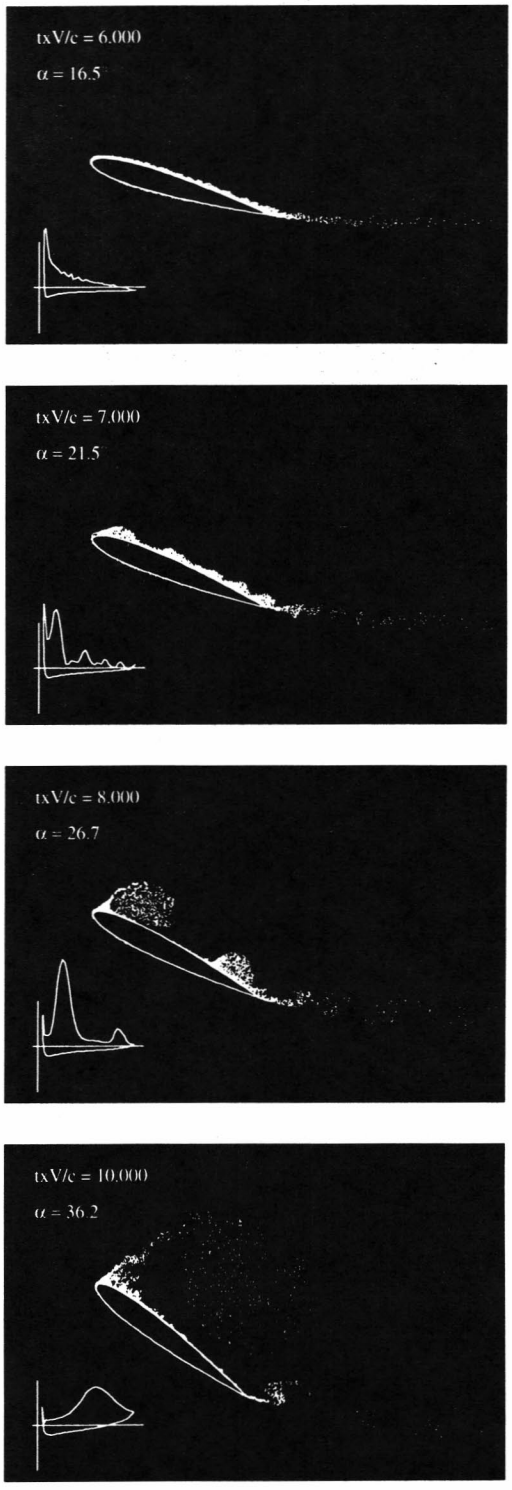

Figure 9. Vortex pattern of the NACA0012 during ramp-up motion

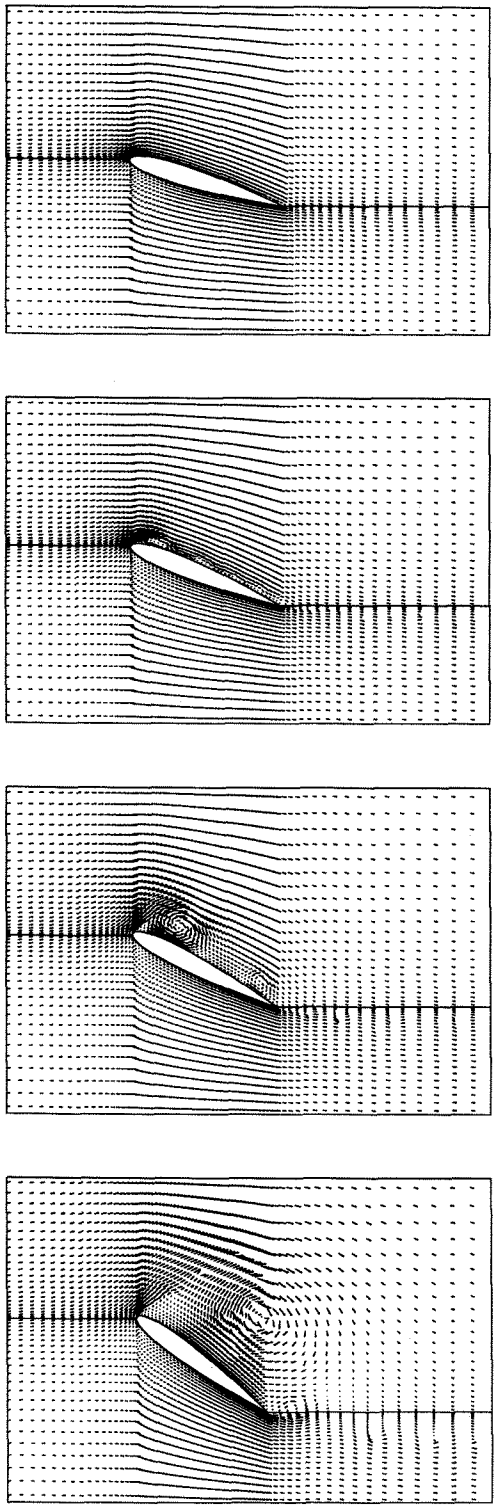

Figure 10. Velocity field of the NACA0012 during ramp-up motion

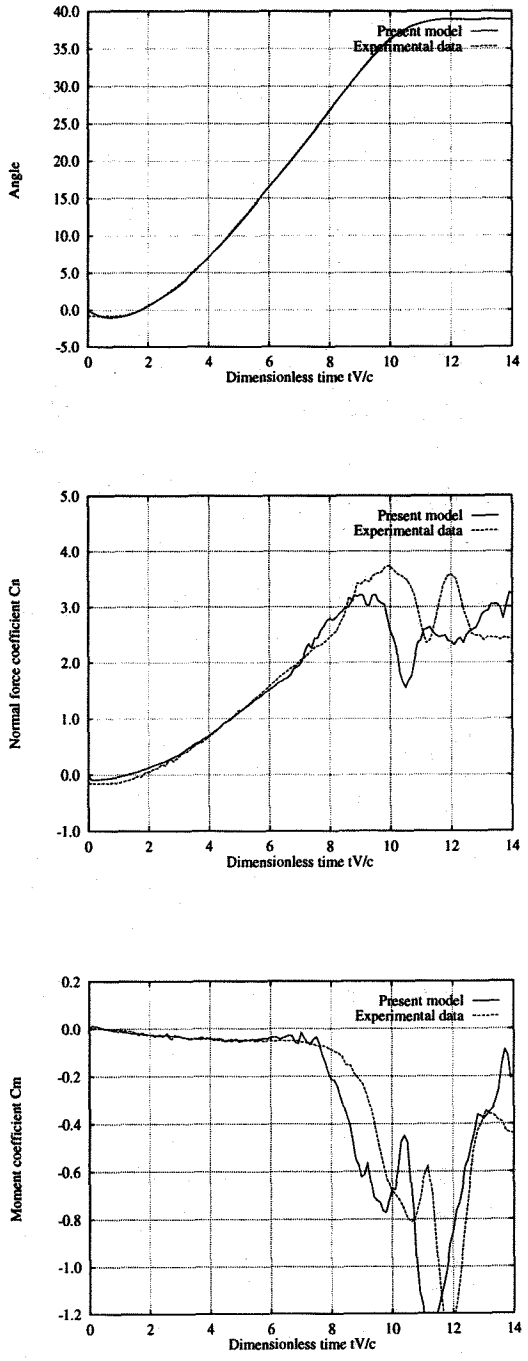

Figure 11. Characteristics for the NACA0012 during ramp-up motion

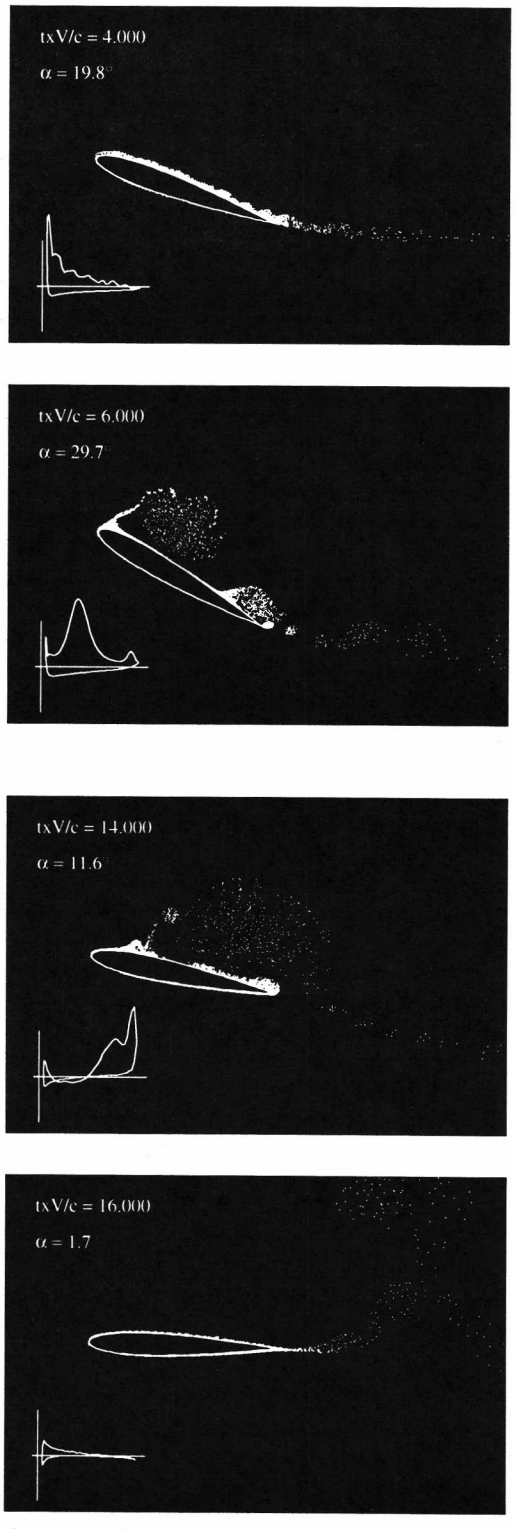

Figure 12. Vortex pattern and pressure distribution of the NACA0012 during ramp up and down

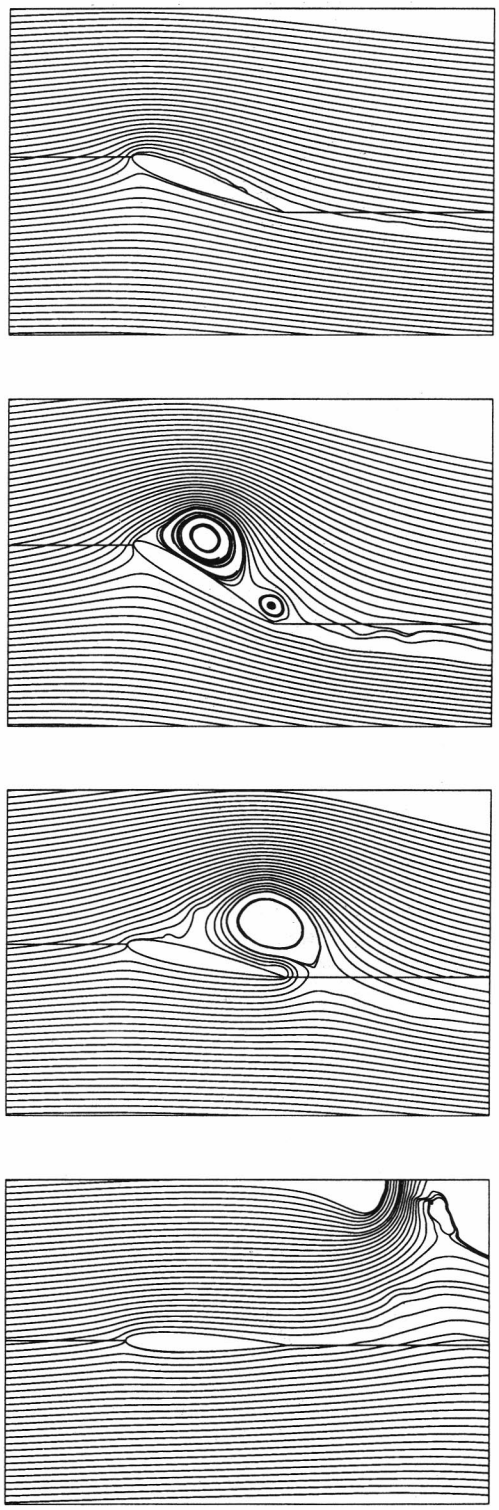

Figure 13. Streamlines around NACA0012 at ramp-up and down

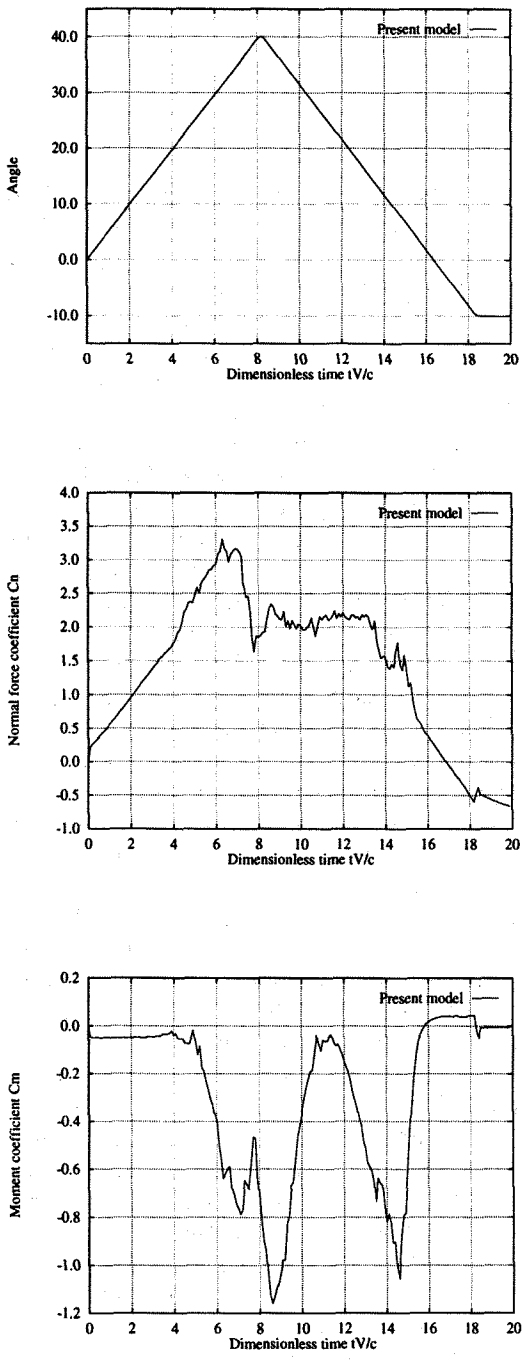

Figure 14. Characteristics for the NACA0012 during ramp up and down